PNAS RESEARCH ARTICLE | MEDICAL SCIENCES

Intraductal administration of transferrin receptor-targeted immunotoxin clears ductal carcinoma in situ in mouse models of breast cancer—a preclinical study

Guannan Wang[a,b,1], Alok Kumar[a,1], Wanjun Ding[a,c,1], Preethi Korangath[a], Tapan Bera[d], Junxia Wei[d], Priya Pai[a], Kathleen Gabrielson[a,e], Ira Pastan[d,2], and Saraswati Sukumar[a,2]

Edited by Myles Brown, Dana–Farber Cancer Institute, Boston, MA; received January 5, 2022; accepted April 29, 2022

The human transferrin receptor (TFR) is overexpressed in most breast cancers, including preneoplastic ductal carcinoma in situ (DCIS). HB21(Fv)-PE40 is a single-chain immunotoxin (IT) engineered by fusing the variable region of a monoclonal antibody (HB21) against a TFR with a 40 kDa fragment of *Pseudomonas* exotoxin (PE). In humans, the administration of other TFR-targeted immunotoxins intrathecally led to inflammation and vascular leakage. We proposed that for treatment of DCIS, intraductal (i.duc) injection of HB21(Fv)-PE40 could avoid systemic toxicity while retaining its potent antitumor effects on visible and occult tumors in the entire ductal tree. Pharmacokinetic studies in mice showed that, in contrast to intravenous injection, IT was undetectable by enzyme-linked immunosorbent assay in blood following i.duc injection of up to 3.0 μg HB21(Fv)-PE40. We demonstrated the antitumor efficacy of HB21(Fv)-PE40 in two mammary-in-duct (MIND) models, MCF7 and SUM225, grown in NOD/SCID/gamma mice. Tumors were undetectable by In Vivo Imaging System (IVIS) imaging in intraductally treated mice within 1 wk of initiation of the regimen (IT once weekly/3 wk, 1.5 μg/teat). MCF7 tumor–bearing mice remained tumor free for up to 60 d of observation with i.duc IT, whereas the HB21 antibody alone or intraperitoneal IT treatment had minimal/no antitumor effects. These and similar findings in the SUM225 MIND model were substantiated by analysis of mammary gland whole mounts, histology, and immunohistochemistry for the proteins Ki67, CD31, CD71 (TFR), and Ku80. This study provides a strong preclinical foundation for conducting feasibility and safety trials in patients with stage 0 breast cancer.

intraductal | immunotoxin | mouse | mammary | tumor

Significance

There is a great need for novel approaches to the treatment of ductal carcinoma in situ, which affects 69,000 women per year in the United States and now requires breast surgery. We have found that intraductal (local) administration of an immunotoxin targeting the human transferrin receptor in mice eliminates breast tumors with no leakage into the blood and no potential systemic toxicity and could provide in the future an alternative to breast cancer surgery.

With the advent of monoclonal antibodies (mAb) in the 1980s, the vision that cell-specific targeted antibodies or antibodies linked to potent plant toxins could achieve tumor-specific killing has become a reality (1, 2). Since then, many immunotoxins (ITs) have been engineered to specifically target cancer cells (3–5).

One of these, HB21(Fv)-PE40, consists of the variable regions of HB21, a monoclonal antibody to the human transferrin receptor (TFR), fused to PE40, a truncated form of *Pseudomonas* exotoxin (PE) A that is devoid of its binding domain and, once internalized, leads to protein translation arrest and cell death (6, 7). Clinical success was achieved with moxetumomab pasudotox (an Fv fragment of an anti-CD22 antibody fused to a truncated 38 kDa PE) for the treatment of hairy cell leukemia (8). In a pivotal trial evaluating 80 patients with relapsed or refractory hairy cell leukemia, the complete response rate was 41% and the overall response rate was 75%. This trial led to FDA approval of moxetumomab pasudotox in 2018 (8) and was followed by additional reports of its clinical effectiveness (4, 9, 10).

The TFR is expressed at markedly higher levels in all subtypes of breast cancer compared to normal breast epithelium (11–14). The most comprehensive study of TFR expression in various breast pathologies was conducted by Singh et al. (12), who reported low-level expression in benign breast lesions ($n = 172$), abundant expression in ductal carcinoma in situ (DCIS) ($n = 65$; > 50% cells) and in invasive breast cancer ($n = 38$; > 80% cells), but negligible expression in normal breast tissue ($n = 127$). This widespread, tumor-specific expression renders TFR a potent target for antibody–toxin conjugates.

A barrier to the systemic use of TFR-directed ITs in the clinic is the known widespread distribution of TFR in many important tissues like the liver and blood vessels that would lead to adverse events. Previously, a conjugate of a monoclonal antibody to the TFR and recombinant ricin A chain (454A12-rRA) was investigated for local treatment of glioblastoma (15). A dose finding toxicity with 454A12-rRA showed that administered

Author affiliations: [a]Department of Oncology, Johns Hopkins University School of Medicine, Baltimore, MD 21287; [b]Lombardi Comprehensive Cancer Center, Georgetown University, Washington, DC 20007; [c]Department of Oncology, Renmin Hospital of Wuhan University, Wuhan, 430060, China; [d]Center for Cancer Research, National Cancer Institute, Bethesda, MD 20892; and [e]Department of Molecular and Comparative Pathobiology, Johns Hopkins University School of Medicine, Baltimore, MD 21205

Author contributions: G.W., I.P., and S.S. designed research; G.W., A.K., W.D., P.K., J.W., P.P., K.G., and S.S. performed research; T.B. and I.P. contributed new reagents/analytic tools; G.W., A.K., W.D., I.P., and S.S. analyzed data; and G.W., A.K., W.D., and S.S. wrote the paper.

The authors declare no competing interest.

This article is a PNAS Direct Submission.

[1]G.W., A.K., and W.D. contributed equally to this work.

[2]To whom correspondence may be addressed. Email: saras@jhmi.edu or pastani@mail.nih.gov.

This article contains supporting information online at http://www.pnas.org/lookup/suppl/doi:10.1073/pnas.2200200119/-/DCSupplemental.

Published June 8, 2022.

intraventricularly, half of the eight patients exhibited temporary tumor responses. No acute or chronic drug toxicity was seen in patients who received up to 38 μg IT. Doses more than or equal to 120 μg caused a cerebrospinal fluid (CSF) inflammatory response that was associated with transient headache, vomiting, and altered mental status that was responsive to steroids and CSF drainage. No systemic toxicity was detected (15). Although promising, many hurdles remain in realizing the potential of local IT treatment in the brain, including inconsistent drug delivery and local toxicity (16).

Based on the high levels of expression of TFR in invasive breast cancer and DCIS, we hypothesized that we can circumvent the problem of systemic toxicity while at the same time control local breast cancer by administering HB21(Fv)-PE40 through the intraductal (i.duc) route. DCIS is a preneoplastic lesion in which the cancer cells are confined within the myoepithelial lining of the mammary ducts (17). Currently, there is concern that many patients with DCIS are overtreated by ablative surgery and radiation (18–20). The consensus opinion is that treatment with minimally invasive procedures should receive serious consideration to improve the quality of life of patients with DCIS (18–20). It is unlikely that surgery will be replaced as a treatment for DCIS, unless a safe and equally effective alternative is provided.

That i.duc therapy shows promise for treating DCIS has been demonstrated in several preclinical studies (21–28). As shown by our group, the superior effects of the i.duc route, compared to the systemic route, for the delivery of chemotherapy (21, 22), radioactive compounds (24), and hormonal agents (18, 21) stems from the ability to confine the anticancer effects of the agent to the tumor site in the duct while sparing the remainder of the body from its toxic effects. We demonstrated the feasibility of and ready acceptance by women of the i.duc route for delivering drugs in a clinical study performed using i.duc Doxil in women prior to surgery (22).

While i.duc chemotherapy (21, 22), radiotherapy (24), and endocrine therapy (21, 26) approaches significantly reduced tumor burden, none of these approaches eradicated tumor cells. As a result, tumors regrew in the animals upon long-term follow-up. In this study, we tested the anticancer efficacy of i.duc administration of HB21(Fv)-PE40 in mammary-in-duct (MIND) models of DCIS using MCF7 and SUM225 (24, 29–31). We show that the i.duc administration of IT rendered 100% of the mice bearing i.duc MCF7 and SUM225 mammary outgrowths tumor free. Unlike intravenous (i.v.) injected IT, no toxin was measurable in the blood of mice by enzyme-linked immunosorbent assay (ELISA) 5 to 30 min after i.duc injection. Compared to current treatments, this approach addresses the ablation of DCIS, both visible and occult, in the entire diseased ductal tree. In addition, unlike i.duc chemotherapy and radiotherapy there is no risk of causing mutations in DNA using ITs. Our findings provide a strong foundation for the potential use of i.duc ITs as a therapeutic approach for DCIS.

Results

The preclinical study design used to test the effectiveness of the recombinant IT, HB21(Fv)-PE40, on stage 0 breast cancer is illustrated in Fig. 1. The IT was tested in the MIND model of breast cancer wherein the injection of luciferase-tagged tumor cells into the fourth mammary gland pair results in the development of DCIS within 1 wk, with or without progression to invasive cancer. The IT is injected into the mammary gland by i.duc administration up to 3 times at weekly intervals accompanied by noninvasive follow-up with In Vivo Imaging System (IVIS) imaging. The IT is internalized through antibody-mediated binding to the abundantly expressed TFR into the tumor cells and is digested in the endosome, causing the release of the PE toxin. The PE toxin causes translation arrest by inactivating elongation factor 2 and induces apoptotic cell death of the tumor cells (32, 33).

Cytotoxic effect of HB21(Fv)-PE40 occurs at very low levels of IT in both ER+ and ER− breast cancer cells. Because of the abundance of the TFR expression in many types of cancer cells, the ability of monoclonal antibodies linked to other molecules to

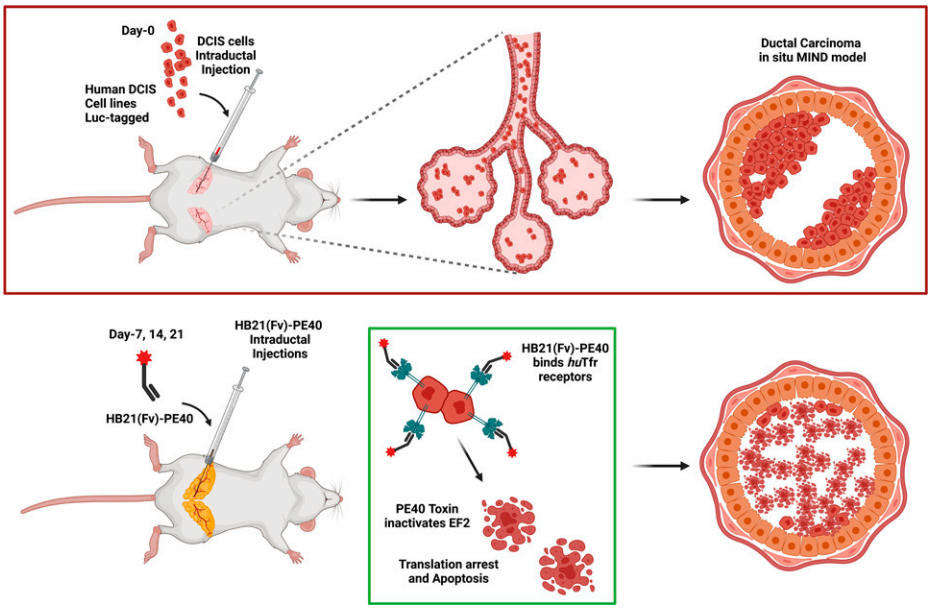

Fig. 1. Study design and mode of action of a recombinant IT in the MIND xenograft tumor model system. Human breast carcinoma (MCF7) or DCIS (SUM225) cells are injected into the right and left teats of parous mice. The cells grow in the duct as in situ lesions. A week later, an IT consisting of the Fv fragment of a human TFR mAb (HB21) fused to a 40 KD fragment of *Pseudomonas* exotoxin, HB21 (Fv)-PE40, is injected on day 7, 14, and 21. The IT binds to the TFR expressed in abundance on breast cancer cells and is internalized, and the released toxin causes translation arrest by inactivating elongation factor 2, EF2, resulting in targeted cell death. This schematic representation was generated using Biorender.com.

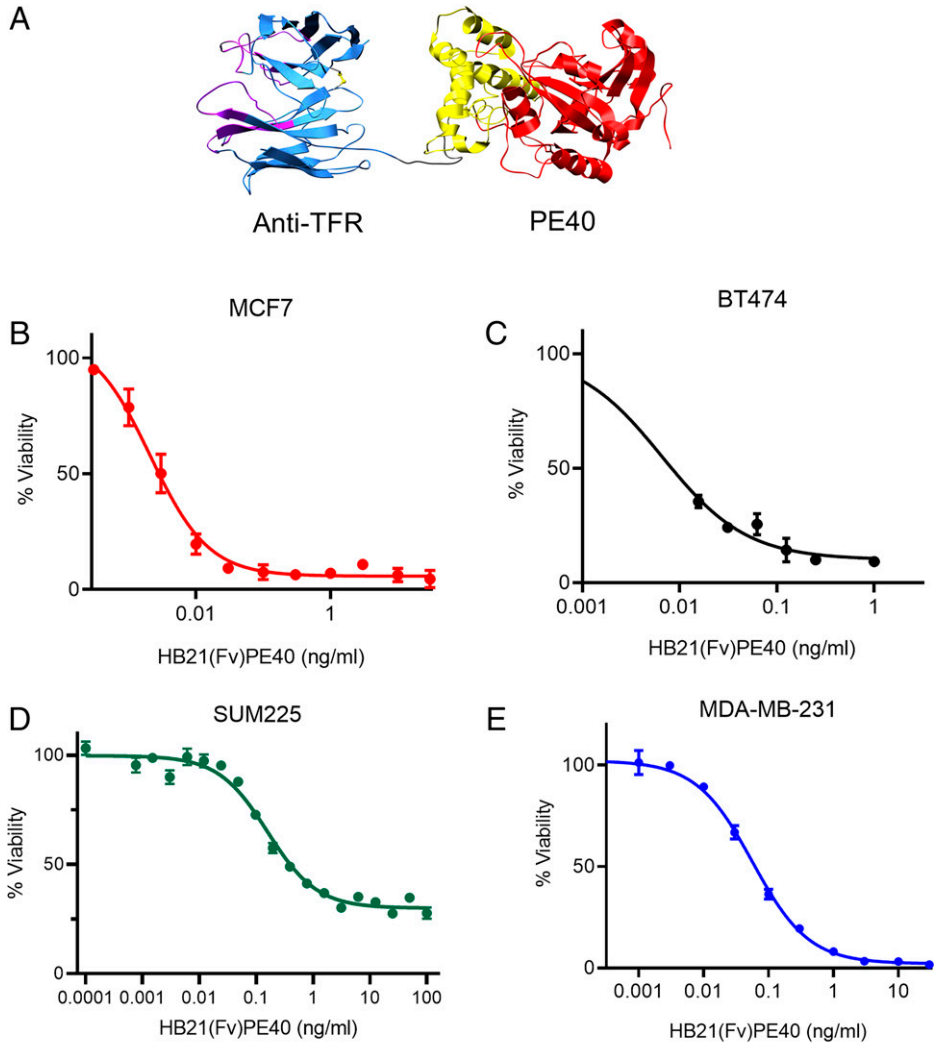

F

Cell line	HB21(Fv)-PE40 IC_{50} ng/ml
MCF-7	0.002085
BT474	0.02216
SUM225	0.1582
MDA-MB-231	0.05664

Fig. 2. Cytotoxicity of the recombinant IT in breast cancer cells. (*A*) Structural domains of the IT. Cytotoxicity of HB21(Fv)-PE40 was tested by the MTS assay in (*B*) MCF7, ER+/PR+ cell line; (*C*) BT474, ER+/PR+/HER2+ cell line; (*D*) the SUM225, ER−/PR−/HER2+ DCIS cell line; and (*E*) MDA-MB-231, ER−/PR−/HER2− or "triple negative" breast cancer cells. Representative graphs are shown. Each assay contained four replicates for each data point, and the assays were repeated 3 times. (*F*) The IC_{50} (ng/mL) of HB21(Fv)-PE40 in each of the four breast cancer cell lines is tabulated. The IC_{50} of MCF7 was the lowest among the four cell lines tested at 0.002 ng/mL, and the IC_{50} of SUM225 was the highest (sevenfold higher than MCF7) at 0.158 ng/mL.

therapeutically target the TFR has been previously tested (34–36). As a first step to assess the cell-killing effects of HB21(Fv)-PE40 in breast cancer, we tested its cytotoxicity in four cell lines of different molecular subtypes: MCF7 (ER+, PR+, HER2−), BT474 (ER+, PR+, HER2+), SUM225 (ER−, PR−, HER2+), and MDA-MB-231 (ER−, PR−, HER2−) using the live-cell MTS (3-(4,5-dimethylthiazol-2-yl)-5-(3-carboxymethoxyphenyl)-2-(4-sulfophenyl)-2H-tetrazolium) assay. The results showed that HB21(Fv)-PE40 (Fig. 2*A*) induced strong antiproliferative effects in all four breast cancer cell lines (Fig. 2 *B*–*E*). IC_{50} (half maximal inhibitory concentration) analysis indicated that the cancer-killing ability of HB21(Fv)-PE40 was in the picomolar to nanomolar levels of the IT, depending on the cell line (Fig. 2*F*). The hormone receptor–positive cell lines MCF7 and BT474 were more sensitive to HB21(Fv)-PE40 (IC_{50} of 0.002 and 0.022 ng/mL, respectively) compared to the ER/PR− breast cancer cell lines SUM225 and MDA-MB-231 (IC_{50} of 0.158 and 0.057 ng/mL, respectively). Thus, HB21(Fv)-PE40 action occurs in the picomolar to nanomolar levels in the tested breast cancer cell lines.

HB21(Fv)-PE40 was undetectable in plasma following i.duc IT administration. Work by us and others (21–24, 26, 37–39) has presented a strong argument for the use of both chemotherapies

and biological therapies by the i.duc route. Due to the abundance of TFR expression in liver cells, we anticipated the hepatic and vascular toxicity of IT administered through the systemic route to humans. To test whether i.duc IT would minimize liver and other toxicities, we determined the pharmacokinetic profiles of the IT following i.duc injection in mice. Since the human TFR-targeted IT does not bind mouse TFR, the level of escape of the IT into the circulation following i.duc injection was measured as an indirect indicator of toxicity. The half-life of the HB21(FV)-PE40 IT in circulation in mice is estimated to be approximately 30 min (34). Based on published literature (35) and our own pilot experiments, we injected 1.0 μg or 3.0 μg HB21(FV)-PE40 by the i.v. route (3 mice each) and collected blood at 5 min, 30 min, and 60 min. The IT was also injected by the i.duc route (3.0 μg total; 1.5 μg/teat/2 teats; 10 mice) for blood collection at 5 min and 30 min thereafter. We determined the concentration of the IT in mouse plasma by ELISA using antibodies to TFR (α-CD71) (40). After i.v. injection, HB21(FV)-PE40 was detected in plasma at each of the three time points (Fig. 3 *A*–*C* and *SI Appendix*, Table S1 *A* and *B* and Fig. S1). However, in all 10 mice receiving i.duc IT, optical density at 450 nm (OD450) values of HB21(FV)-PE40 in the plasma samples at both 5 min and 30 min were below 10 ng/mL, which is the limit of detection of TFR by ELISA (Fig. 3*C* and *SI Appendix*, Table S2 *A* and *B*). In all likelihood, the safety profile of the i.duc drug will be significantly enhanced, resulting in low and manageable levels of toxicity.

MIND MCF7–DCIS-like tumors are undetectable after i.duc treatment of mice with HB21(Fv)-PE40. Next, we tested the antitumor effects of HB21(Fv)-PE40 in two MIND models of DCIS (26, 29, 31). In the MCF7 model, DCIS lesions form inside the mammary ducts within 1 wk after i.duc injection of 2×10^5 tumor cells, which progress to invasive cancer by 3 wk (26). Mice received i.duc injections of tumor cells on day 0. Tumor-bearing mice (confirmed by IVIS imaging) received bilateral i.duc injections of 15 μL vehicle (0.2% HSA in PBS) or 1.5 μg IT (total 3.0 μg per mouse), or 3.0 μg IT through the intraperitoneal (i.p.) route on days 7, 14, and 21 (schema in Fig. 4*A*). Tumor volume was monitored by IVIS imaging at weekly intervals. Compared to i.duc vehicle, HB21(Fv)-PE40 administered through the i.p. route inhibited MCF7 tumor growth, but tumor recurrence was observed upon cessation of treatment at approximately day 26 (Fig. 4 *B* and *C*). On the other hand, mice that received i.duc HB21(Fv)-PE40 had no detectable tumors by IVIS imaging within 2 wk following the completion of 2/3 treatments. No recurrence was detected even after 61 d of follow-up (Fig. 4 *B* and *C*). On day 32, we killed two mice from each group to examine the four mammary glands by carmine staining of the whole mount and hematoxylin and eosin (H & E) staining of formalin-fixed paraffin-embedded (FFPE) sections. Dense mammary glands (whole mount) were seen in the vehicle-treated group (Fig. 4 *D*, *a*, *b*). Remarkably, in the i.duc group, histopathological examination of H & E–stained slides of the mammary glands of the IT-treated mice revealed the absence of tumor cells (Fig. 4*E*), consistent with the findings by IVIS imaging (Fig. 4 *B* and *C*) and an architecture consistent with a normal mammary gland. Immunohistochemical (IHC) analysis of the vehicle-treated mammary glands showed the presence of highly proliferative Ki67+ tumors (Fig. 4*F*), with abundant microvasculature

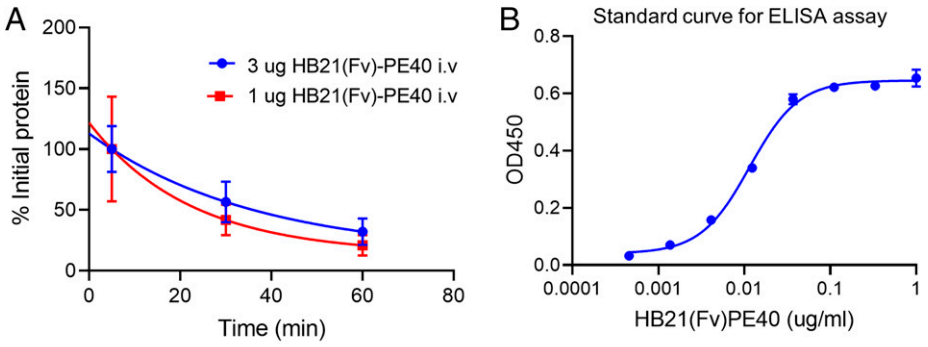

C

	HB21(Fv)PE40 (ug/ml of plasma) / time			
Number of mice	Dose/route	5 min	30 min	60 min
3	3 ug i.v	1.49	0.71	0.39
		2.18	1.2	0.8
		2	1.3	0.63
3	1 ug i.v	0.52	0.22	0.12
		0.9	0.34	0.18
		0.4	0.2	0.08
10	3 ug i. duc	<10 ng/ml*	<10ng/ml*	-

* Below the range of detection by ELISA

Fig. 3. Pharmacokinetics of HB21(Fv)-PE40 in mice. Female immunodeficient mice received i.v. injections of 3.0 μg (3 mice) or 1.0 μg of HB21(Fv)-PE40 (3 mice) through the tail vein. Blood samples were drawn at 5, 30, and 60 min. Next, 10 age-matched female NSG mice received i.duc injections of 1.5 μg per teat of HB21(Fv)-PE40 into two fourth-pair mammary glands (total 3.0 μg/mouse). Blood samples were drawn at 5 and 30 min. (*A*) The level of IT in mouse plasma as measured by ELISA is plotted against time in minutes. (*B*) The standard curve of different dilutions of the IT, determined at OD450, was used to calculate drug levels in plasma. (*C*) The experimental design and level of IT in the plasma (estimate of 1.1 to 1.6 mL total plasma/per mouse) as determined by ELISA is tabulated. *denotes TFR levels below range of detection by ELISA. *SI Appendix*, Tables S1 and S2 provide supportive information for plasma levels following i.v. and i.duc injection of the IT.

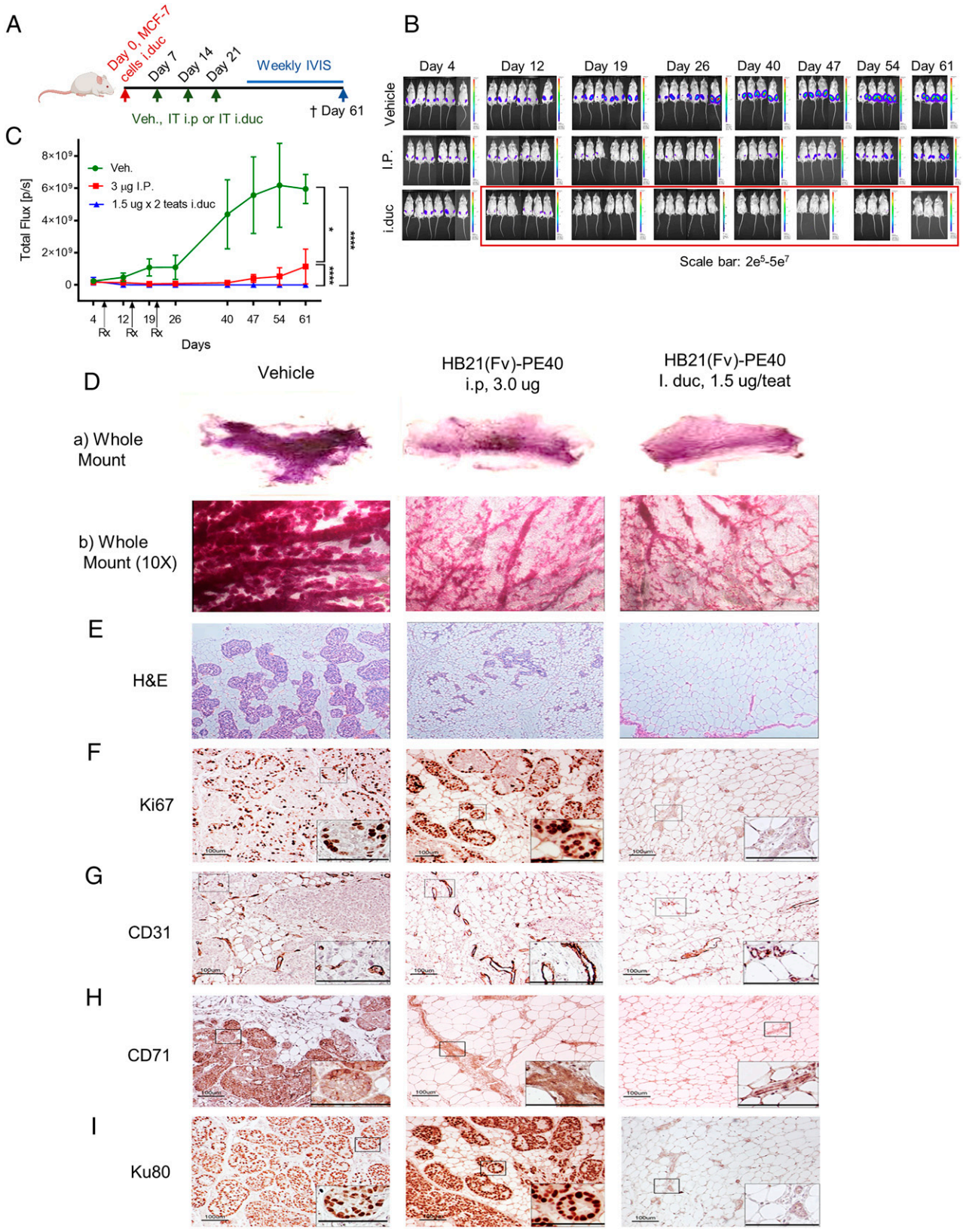

Fig. 4. I.duc but not i.p. delivery of the TFR-directed IT, HB21(Fv)-PE40, eliminates tumors in the MCF7 MIND model of breast cancer. (*A*) A schematic of the i.duc tumor cell injection and treatment schedule with follow-up. (*B*) Tumor burden and progression by IVIS imaging. (*C*) Quantification of tumor growth as photons per second over time. Figure shows that mice that received 1.5 µg/teat i.duc IT showed complete lack of signal within 7 d of injection, mice that received 0.15 µg IT per teat tumor were cleared by 14 d, and the HB21 mAb alone had no significant change in size compared to mice in the vehicle control group; $*P < 0.05$, $***P < 0.001$ (Scale bar, $5e^6$–$5e^8$). Red box indicates that a lower scale of $2e^5$–$5e^7$ was used for the IT-treated groups to enable the detection of small signals. (*D*) Carmine staining of (*a*) whole mounts of mammary glands (*b*) viewed at 10 X. (*E*) H & E staining of FFPE sections of mammary glands. IHC analysis for (*F*) Ki67 (proliferation), (*G*) CD31 (blood vessels), (*H*) CD71 (human TFR) and (*I*) human Ku80 shows that the ducts were filled with proliferating tumor cells, often invasive, with abundant neo-vasculature, and TFR+ tumor cells of human origin (Ku80) were present in the vehicle- and HB21-mAb–treated groups, with significantly reduced (0.15 µg/teat) or no evidence of tumor cells (1.5 µg/teat) in the IT-treated groups, resulting in a mammary gland structure similar to the mammary gland in a normal mouse (Scale bar, 100 µm).

positive for CD31 (Fig. 4*G*). More important, the tumors showed abundant TFR/CD71 expression (Fig. 4*H*), indicating the presence of human tumor cells. A striking reduction in all these markers was observed in both i.p. and i.duc IT–treated mice (Fig. 4 *D*–*H*). Finally, human Ku80 staining confirmed the human origin of these tumors and ruled out the development of spontaneous tumors in the control groups (Fig. 4*I*). While residual tumors by H & E and IHC signals for the tested proteins were observed in the i.p. IT–treated mice, all the mammary glands in the i.duc-treated group remained tumor free with a completely cleared mammary gland tree. Similar analysis of the remaining mice after 61 d of follow-up showed invasive tumors in the vehicle group, small tumors in the i.p. IT–treated group, and no tumors upon gross and microscopic examination in the i.duc IT–treated group, similar to those shown in Fig. 4 *D*–*I*. Thus, i.duc treatment of mice with DCIS lesions resulted in a pathologic complete response that lasted through the observation period of 61 d.

In a second experiment with the MCF7 MIND model system, we tested the antitumor effects of i.duc treatment using a 1/10th lower dose of HB21(Fv)-PE40 (0.15 μg/teat × 2 teats) and the previously tested dose (1.5 μg/teat × 2 teats), using both the HB21 mAb (41) alone (1.5 μg/teat × 2 teats), and the i.duc vehicle-treated groups as controls (*SI Appendix*, Fig. S2 *A*–*C*). Following the same schedule as the previous experiment, treatment was initiated 1 wk after tumor cell injection and was performed 3 times at weekly intervals. Once again, 1.5 μg IT per teat resulted in tumor signal elimination within 1 wk (*SI Appendix*, Fig. S2 *B* and *C*). At 30 d of observation, small signals remained in the 0.15 μg IT/teat–treated group as measured by IVIS imaging (*SI Appendix*, Fig. S2*B*). The HB21 mAb alone did not inhibit tumor growth (*SI Appendix*, Fig. S2 *B* and *C*). Mice in the vehicle and mAb control groups were killed at day 48. Carmine staining of whole mounts showed a high level of tumor burden inside the mammary glands from the control groups (*SI Appendix*, Fig. S2 *D*, *a*, *b*). The mice in the 0.15 μg and 1.5 μg dosage group were followed up to 143 d by palpation, but not by IVIS, due to COVID-19–mandated restrictions. As shown in *SI Appendix*, Fig. S2 *E*–*I* for representative mice, the 1.5 μg/teat IT–treated mammary glands remained tumor free and resembled normal mammary glands for all the proteins examined by IHC: Ki67, CD31, CD71, and Ku80. In the 0.15 μg IT/teat–treated group, small nests of residual tumors were observed inside the mammary ducts (*SI Appendix*, Fig. S2 *E*–*I*). The quantitation of signals, performed using Q-Path (42), ImageScope (43), or ImageJ (44), showed highly significant differences for Ki67, CD31, and CD71 in vehicle- and IT-treated tumors (*SI Appendix*, Fig. S2 *J*–*M*). Human Ku80 staining and its quantitation by ImageJ supported the absence of signals from human breast cancer cells in the 1.5 μg/teat IT-treated mouse mammary glands as shown in *SI Appendix*, Fig. S2*M*. Thus, we concluded that the IT, even at a low dose of 1.5 μg/teat, was potently effective in the elimination of cancer cells in the duct.

HB21(Fv)-PE40 i.duc has potent antitumor effects in SUM225 DCIS in mice. Nearly 80% of DCIS are ER+/PR+ (45). In addition, approximately 30% of DCIS tumors express HER2 (45). We tested the effect of HB21(Fv)-PE40 in SUM225-Luciferase tagged i.duc xenografts, representative of ER−/PR−, HER2+ DCIS. We injected 1×10^5 SUM225-Luc cells by the i.duc route to establish the MIND model of HER2+ DCIS. A pilot experiment was conducted (study design in *SI Appendix*, Fig. S3*A*) that showed the clearance of SUM225 tumors as early as 2 wk of i.duc treatment with 1.5 μg IT by IVIS imaging. No recurrence was observed until the termination of the experiment on day 48 (*SI Appendix*, Fig. S3 *B* and *C*). A second experiment (schema in *SI Appendix*, Fig. S3*D*) tested the same dose and a 1/10th dose of i.duc IT, with vehicle-injected mice as controls ($n = 7$ mice/group). As shown in *SI Appendix*, Fig. S3 *E* and *F*, the majority of the mammary glands (11/14) were tumor free after i.duc treatment with HB21(Fv)-PE40 (1.5 μg/teat), but weaker antitumor effects were observed at the lower dose (0.15 μg/teat). Upon higher IVIS exposure (red box in *SI Appendix*, Fig. S3 *F*), residual tumor signals were observed in the low-dose group and small signals were observed in the high-dose group as well at day 35 of observation (*SI Appendix*, Fig. S3 *E* and *F*). The results of the final replicate testing the effectiveness of the IT in this model are shown in Fig. 5. Using a study design shown in Fig. 5*A*, IVIS imaging (Fig. 5*B*) and its quantitation during follow-up (Fig. 5*C*) showed that SUM225 cells grow aggressively at the in-duct location. Here, HB21 mAb treatment promoted growth, although not significantly (Fig. 5 *B* and *C*) compared to vehicle control. Aggressive growth of the SUM225 cells occurred; the entire ductal structure was filled with tumor cells to cause thickness and opaqueness in the whole mount (Fig. 5*D* and *SI Appendix*, Fig. S4*A*). Histopathology following H & E staining confirmed the almost complete replacement of the mammary gland with large islands of tumor lesions that maintained their DCIS pathology with no invasion past the myoepithelial cells of the duct. Meanwhile, significant central necrosis (comedo-necrosis) was seen within the involved ducts (Fig. 5*E*). This is consistent with a type of high-grade DCIS in patients called comedo-carcinoma, which is also frequently associated with HER2 overexpression (46). Ki67 staining confirmed the presence of proliferating cells (Fig. 5*F*), CD31 staining showed their neo-microvasculature (Fig. 5*G*), CD71 staining showed the high levels of expression of the human TFR (Fig. 5*H*), and Ku80 staining confirmed the human origin of the tumor cells (*SI Appendix*, Fig. S4 *B* and *C*). HB21 mAb treatment had little effect on all the markers, while low-dose IT showed a significant effect of tumor reduction as reflected in the tumor growth curve (Fig. 5*C*) and in the H & E sections (Fig. 5*E*). Similar, highly significant reduction or elimination of immunoreactivity was seen for CD31, CD71, and Ku80 (Fig. 5 *F*–*H* and *SI Appendix*, Fig. S4*B*), quantitated in Fig. 5 *I*–*K* and in *SI Appendix*, Fig. S4*C*. Thus, we have shown in a second MIND model of an HER2+ DCIS SUM225 that IT is very effective in reducing and in some cases eliminating tumor cells despite the aggressiveness of the tumor cells.

Discussion

The widespread use of mammographic screening has increased the frequency of diagnosis of DCIS significantly. In the United States, 18 to 25% of new diagnosed breast cancers are DCIS (47). The rationale for treating DCIS aggressively is to prevent its progression into invasive breast cancer. However, due to a lack of the precise prediction of its fate to an invasive lesion, the standard treatment for almost all patients diagnosed with DCIS is local surgery and adjuvant radiation (38, 48). We and others have shown that i.duc therapy provides a noninvasive modality to treat DCIS at the site of origin. Several types of antitumor agents, including hormone therapy, chemotherapy, and radiotherapy have been investigated in preclinical research (21, 22, 24–28), and a safety and feasibility clinical trial was successfully conducted with Doxil administered by the i.duc route (22). The results are promising overall, but problems still

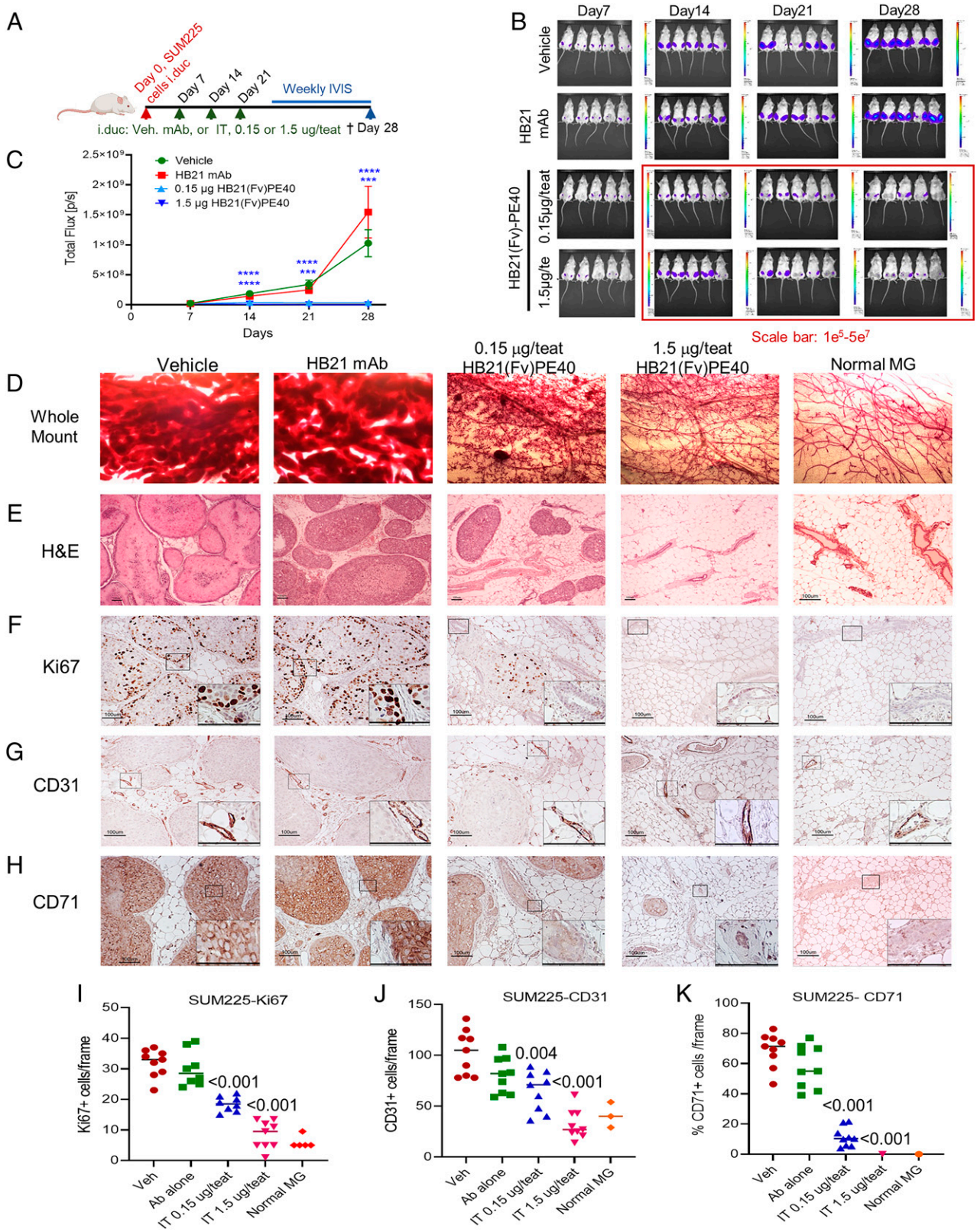

Fig. 5. Highly significant reduction of tumor burden is achieved in the SUM225-DCIS model of breast cancer by i.duc delivery of the TFR-directed IT, HB21(Fv)-PE40. (*A*) A schematic of the i.duc tumor cell injection and treatment schedule with follow-up. (*B*) Tumor ($n = 20$ per group) burden and progression by IVIS imaging. The scale used was $2e^6$–$5e^8$; the red box indicates that a lower scale of $1e^5$–$5e^7$ was used for the IT-treated groups to enable the detection of small signals. (*C*) Quantification of tumor growth as photons per second over time. Figure shows that mice that received 0.15 µg or 1.5 µg/teat i.duc IT had very low to absent signals by the end of the experiment. ***$P < 0.001$, ****$P < 0.0001$. At the end of the experiment, tissues from three mice/group were examined histologically. (*D*) Low-magnification images of mammary gland whole mount compares gross morphology in the vehicle- and mAb-treated groups show dense filling of all the ductal branches compared to low- and high-dose IT-treated groups that resemble normal mammary glands. (*E*) H & E staining of FFPE sections of mammary glands. IHC for (*F*) Ki67 (proliferation), (*G*) CD31 (blood vessels), and (*H*) CD71 (human TFR) 2 wk after initiation of treatment (Scale bar, 100 µm). (*I*–*K*) IHC staining of FFPE sections of tumors from three mice in three predetermined regions per slide was quantitated using Q-Path, ImageScope, and ImageJ (Fiji). Both Kruskal–Wallis (between group comparisons) and Mann–Whitney comparisons with the vehicle group were performed. Mann–Whitney *P* values are indicated in the graph. MG, mammary gland.

exist, such as suboptimal antitumor efficiency of endocrine agents (26) and long-term effects of DNA-damaging agents such as chemotherapy and radiotherapy (49). Treatment using biological agents such as antibodies or antibody-targeted protein toxins may circumvent these problems. In this paper, we describe one such strategy.

PE-based toxins have high cell-killing activity, a well-understood mechanism of action, and the ability to endure many mutations without compromising the toxin's activity (6). By conjugation to tumor-specific monoclonal antibodies, deadly toxins are accurately delivered into cancer cells expressing those antigens. However, due to cross-reactivity with other essential cells in the body expressing the same antigen, adverse side effects are observed in patients, such as those receiving local intrathecal treatment for gliomas (15). I.duc delivery may overcome this drawback of systemic toxicity. In our study we selected HB21(Fv)-PE40, which is a recombinant IT that targets cells that express the TFR. Iron is essential for cell growth and division. As the regulator of iron import, TFR is overexpressed in many cancer cells, including breast cancer (50). We tested its potential utility in the treatment of DCIS in this study.

Our in vitro MTS assay results suggested the antiproliferative ability of ITs in the picomolar to nanomolar scale in ER+ MCF7 and BT474 cells, ER− HER2+ SUM225, and in triple-negative MDA-MB-231 cells. The experiments in the MIND mouse model also indicated that MCF7-derived DCIS tumors were more sensitive than SUM225-derived DCIS tumors to the IT treatment. Western blot data from Wei Wang et al. (51) showed higher levels of TFR in ER+ (MCF7, T47D) than ER− (MDA-MB-231, MDA-MB-453) cell lysates. Work by Singh et al. on the largest cohort of patients analyzed thus far suggested higher TFR expression in later stages and in higher grades of breast cancer (12). By IHC, expression of TFR was similar in the two cell lines we used in these studies (Figs. 4 and 5). However, our IC_{50} studies in cultured cell lines, although limited, showed differential toxicity among the two cell lines. ER+ MCF7 was highly susceptible (IC_{50}: 0.0020 ng/mL) compared to HER2+ SUM225, which was nearly eightfold less susceptible (IC_{50}: 0.0158 ng/mL) (Fig. 2). This differential susceptibility was also reflected in the in vivo long-term response of the tumors treated by the i.duc route (Figs. 4 and 5 and *SI Appendix*, Figs. S2–S4) with the IT. It is important to note that DCIS with focal invasion tends to be ER− and HER2+ (19). In light of this information, the highly significant antitumor response observed using the IT with the aggressively growing SUM225 MIND model is quite remarkable.

Histology findings on the treated tumors were consistent with gross morphological observations through mouse IVIS imaging and mammary gland whole mount analysis (Figs. 4 and 5). In mice with MCF7 cells growing in the ducts, H & E staining showed a normal mammary gland structure in several sections of each gland from i.duc IT–treated mice, even after long-term follow-up of more than 2 months, in contrast to tumors treated by the i.p. route with IT at the same dose (Fig. 4) or with the HB21 mAb to the TFR (*SI Appendix*, Fig. S2). Quantified using online imaging tools of ImageJ, ImageScope, and Q-Path, near-normal signals were achieved by high-dose ITs in both animal model systems. Sustained antitumor effects were observed in the MCF7 model for up to 143 d of follow-up (Figs. 4 and 5 and *SI Appendix*, Figs. S2, S3, and S5).

Mice tolerated the IT and showed no side effects from the toxin or the mode of injection (Figs. 2 and 3 and *SI Appendix*, Tables S1 and S2). This was predictable since the IT is directed to the human TFR and has no cross-reactivity with the mouse TFR. Pharmacokinetics assays to evaluate how much of the toxin escapes from the mammary gland showed that TFR in the blood was in the undetectable range by ELISA, 5 or 30 min after i.duc injection of HB21(Fv)-PE40. To some extent, these findings suggest the likelihood of a low risk of side effects in clinical translation. This question remains to be resolved by a stepwise dose escalation clinical study of the IT administered by the i.duc route, similar to the study we conducted using pegylated doxorubicin (22).

Despite these highly promising results, some challenges remain in the clinical translation of these findings. Our understanding of breast anatomy is poor. Investigators have identified from as few as five to as many as 27 ductal systems in the breast (38, 52–54), but there is agreement that most breasts contain 5 to 9 main nonanastomosing ductal systems that end in orifices at the nipple; these orifices are generally arranged as a central group and a peripheral group. While cannulation of the affected duct through the easily identifiable nipple orifice for ductoscopy of the breast is routine in women with pathological nipple discharge, predicting which opening at the nipple leads to the ductal system harboring the cancer lesion is difficult. Success rates reported by experienced investigators has been approximately 50% (38). Successful access to and i.duc injection of chemotherapy into 5 to 8 ducts per patient was also reported (54). In our previous feasibility and pegylated doxorubicin dose-determining study, successful cannulation and instillation into one duct was achieved in 15/17 patients; however, in that study, reaching the cancerous duct was not a priority (22). Further studies on the anatomy of the normal human breast to map the location of the orifices at the nipple-bearing ductal system are needed.

Since most low-grade DCIS will not progress, active surveillance and hormone therapy are currently recommended (18–20). However, larger lesions are often treated with more aggressive therapy (55, 56). This larger and higher-grade DCIS may be the lesions where i.duc instilling of IT would be most beneficial. We propose that this intervention could be tested and moved forward in a safe fashion in women with larger DCIS lesions who normally undergo mastectomy since they cannot be resected with breast conservation (55, 56). This intervention could be tested preoperatively, and postmastectomy, the duct could be marked with India ink to enable detailed histological examination of the entire ductal tree. This would allow us to determine whether the duct with the DCIS can be defined and cannulated, whether the intervention causes cell death in the lesion, and its effects on the surrounding tissue.

In summary, we have tested the potency of HB21(Fv)-PE40 administered i.duc in the treatment of DCIS in two preclinical models. These findings are very promising and support the initiation of feasibility, safety, and dose-finding studies in a phase 1/2 clinical trial in patients with stage 0 breast cancer.

Materials and Methods

Detailed materials and methods are presented in *SI Appendix*.

Cell Lines and Reagents. Cultured MCF7-Luc (DMEM, 10% FBS), SUM225-Luc (DMEM/F12; 5% FBS, insulin 10 μg/mL, hydrocortisone 0.5 μg/mL), MDA-MB-231, and BT474 (DMEM; 10% FBS, Corning Cellgro) were used. The cell lines were authenticated within the last 1 y. The IT, HB21(Fv)-PE40, and the anti-TFR mAb, HB21, were generated in the Pastan Laboratory (National Cancer Institute, Bethesda, MD). Human serum albumin, 0.2% in PBS (HSA, Grifols Biologicals LLC, NDC 68516–5216-1) was used to dilute the IT and HB21 and was used as the vehicle control.

MTS Cell Viability Assay. MCF7-Luc and SUM225-Luc cells (5,000 cells/well) were seeded in triplicate in 100 μL cell culture medium in a 96-well plate and incubated overnight. The cells were treated with 200 μL serial dilutions of HB21(Fv)-PE40 toxin diluted in 0.2% HSA in PBS for 72 h. Cells were tested by the MTS cell proliferation assay 48 and 72 h after adding the IT, per the manufacturer's instructions. Absorbance at 490 nm was recorded. Triplicates were averaged for a mean absorbance, and then the percentage survival of IT-treated cells versus time-matched vehicle-treated cells was plotted. Experiments were performed in triplicate.

Mouse Models of DCIS. Animal experiments were conducted following protocols approved by IACUC (Institutional Animal Care and Use Committee) of Johns Hopkins University and the National Cancer Institute, and the animals were handled according to institutional guidelines. Female ex-breeder NOD/SCID/gamma (NSG) mice ~age 8 mo were used. For MIND models, tumor cells in 10 μL serum-free medium (2×10^5 MCF7-Luc or 1×10^5 SUM225-Luc cells) were injected by the i.duc route into each of the two (fourth pair) mammary glands through the teat (26). Mice received i.duc treatment 3 times at weekly intervals, as indicated in the treatment schema.

Tumor Treatment and Monitoring by IVIS Imaging. IVIS imaging was conducted as described (26). Tumor growth was monitored by IVIS imaging at weekly intervals. To compare tumor volume between groups, regions of interest (ROI) were manually selected in tumor-bearing areas, including the whole body. Total flux (photons/second) was measured corresponding to each ROI. All total fluxes were used for statistical analysis. Results of total flux in the tumor against days of follow-up were plotted.

Pharmacokinetics of i.v. and i.duc Administration of HB21(Fv)-PE40. Immunodeficient female mice (ages 6 to 8 wk, Nu/nu) received 1 μg or 3 μg i.v. HB21(Fv)-PE40 through the i.v. route ($n = 3$), Blood samples were collected from the tail vein 5 min, 30 min, and 60 min after IT injection. Age-matched female NSG mice ($n = 10$) received 3 μg i.duc IT (1.5 μg; 2 mammary glands/mouse). Blood was collected at 5 min and 30 min following IT injection from the submandibular vein. IT levels were measured by ELISA. The concentration of IT in plasma was calculated based on the standard curve using a sigmoidal equation in GraphPad Prism version 7.01.

Histopathology. Whole mounts of the mammary glands and FFPE sections were prepared after dissection. Tissue fixation, paraffin-embedding, and H & E staining was done according to standard procedures in the Surgical Pathology Laboratory at Johns Hopkins Hospital.

IHC Staining and Scoring. IHC analysis was performed with primary monoclonal antibodies at the indicated dilutions following antigen retrieval: anti-Ki67 (1:300, Cell Signaling, D2H10), anti-Ku80 (1:300, Cell Signaling, C48E7), anti-CD31 (1:60, Dianova GmbH, DIA-310), and anti-CD71 (1:50, Sigma-Aldrich, MRQ-48). Scoring of the number of positive nuclei (Ki67 and Ku80) was performed using Q-Path (42). CD31+ blood vessels were counted using the positive pixel count algorithm embedded in the APERIO ImageScope software (Leica Biosystems) (43), and CD71+ (TFR+) areas of tumor were quantified using ImageJ (Fiji) (44).

Statistical Analysis. Quantitative data are shown as mean ± SD. A one-way ANOVA was used to compare the difference between groups. The Kruskal–Wallis test was performed to compare the number of positively immunostained cells or tumor areas in treated tumors and normal mammary glands for the four IHC stains. Graphs were drawn and statistical analyses were performed using the GraphPad Prism 7 software. Differences were considered significant if $P < 0.05$.

Data Availability. The data are freely shared upon publication. No code or other data are involved. All study data are included in the article and/or *SI Appendix*.

ACKNOWLEDGMENTS. This work was supported by grants from the Janine Goebel Fund, the Fetting Fund for Breast Cancer Prevention, and the Rubenstein Family Fund to S.S. Open access license has not been selected.

1. K. Strebhardt, A. Ullrich, Paul Ehrlich's magic bullet concept: 100 years of progress. *Nat. Rev. Cancer* **8**, 473–480 (2008).
2. Y. Bordon, The many sides of Paul Ehrlich. *Nat. Immunol.* **17**, S6 (2016).
3. P. Wolf, U. Elsässer-Beile, Pseudomonas exotoxin A: From virulence factor to anti-cancer agent. *Int. J. Med. Microbiol.* **299**, 161–176 (2009).
4. R. J. Kreitman, I. Pastan, Development of recombinant immunotoxins for hairy cell leukemia. *Biomolecules* **10**, 1140 (2020).
5. F. Shafiee, M. G. Aucoin, A. Jahanian-Najafabadi, Targeted diphtheria toxin-based therapy: A review article. *Front. Microbiol.* **10**, 2340 (2019).
6. I. Pastan, R. Hassan, D. J. Fitzgerald, R. J. Kreitman, Immunotoxin therapy of cancer. *Nat. Rev. Cancer* **6**, 559–565 (2006).
7. M. Michalska, P. Wolf, Pseudomonas exotoxin A: Optimized by evolution for effective killing. *Front. Microbiol.* **6**, 963 (2015).
8. R. J. Kreitman *et al.*, Moxetumomab pasudotox in relapsed/refractory hairy cell leukemia. *Leukemia* **32**, 1768–1777 (2018).
9. T. Robak, A. Janus, K. Jamroziak, E. Tiacci, R. J. Kreitman, Vemurafenib and rituximab in patients with hairy cell leukemia previously treated with moxetumomab pasudotox. *J. Clin. Med.* **10**, 2800 (2021).
10. I. R. Yurkiewicz, S. Coutre, H. Ghesquieres, I. Pastan, R. J. Kreitman, Moxetumomab pasudotox as re-treatment for heavily-pretreated relapsed hairy cell leukemia. *Leuk. Lymphoma* **62**, 2812–2814 (2021).
11. F. Wrba, E. Ritzinger, A. Reiner, J. H. Holzner, Transferrin receptor (TrfR) expression in breast carcinoma and its possible relationship to prognosis. An immunohistochemical study. *Virchows Arch. A Pathol. Anat. Histopathol.* **410**, 69–73 (1986).
12. M. Singh *et al.*, Differential expression of transferrin receptor (TfR) in a spectrum of normal to malignant breast tissues: Implications for in situ and invasive carcinoma. *Appl. Immunohistochem. Mol. Morphol.* **19**, 417–423 (2011).
13. L. D. Miller *et al.*, An iron regulatory gene signature predicts outcome in breast cancer. *Cancer Res.* **71**, 6728–6737 (2011).
14. S. Pizzamiglio *et al.*, Expression of iron-related proteins differentiate non-cancerous and cancerous breast tumors. *Int. J. Mol. Sci.* **18**, 410 (2017).
15. D. W. Laske *et al.*, Intraventricular immunotoxin therapy for leptomeningeal neoplasia. *Neurosurgery* **41**, 1039–1049 (1997).
16. J. H. Sampson *et al.*, Intracerebral infusion of an EGFR-targeted toxin in recurrent malignant brain tumors. *Neuro-oncol.* **10**, 320–329 (2008).
17. S. R. Lakhani, The transition from hyperplasia to invasive carcinoma of the breast. *J. Pathol.* **187**, 272–278 (1999).
18. E. S. Hwang *et al.*, The COMET (Comparison of Operative versus Monitoring and Endocrine Therapy) trial: A phase III randomised controlled clinical trial for low-risk ductal carcinoma in situ (DCIS). *BMJ Open* **9**, e026797 (2019).
19. L. L. Visser *et al.*, Predictors of an invasive breast cancer recurrence after DCIS: A systematic review and meta-analyses. *Cancer Epidemiol. Biomarkers Prev.* **28**, 835–845 (2019).
20. S. J. Schnitt, Diagnosis of ductal carcinoma in situ in an era of de-escalation of therapy. *Mod. Pathol.* **34**, 1–7 (2021).
21. S. Murata *et al.*, Ductal access for prevention and therapy of mammary tumors. *Cancer Res.* **66**, 638–645 (2006).
22. V. Stearns *et al.*, Preclinical and clinical evaluation of intraductally administered agents in early breast cancer. *Sci. Transl. Med.* **3**, 106ra108 (2011).
23. A. Brock *et al.*, Silencing HoxA1 by intraductal injection of siRNA lipidoid nanoparticles prevents mammary tumor progression in mice. *Sci. Transl. Med.* **6**, 217ra2 (2014).
24. T. Yoshida *et al.*, Effective treatment of ductal carcinoma in situ with a HER-2- targeted alpha-particle emitting radionuclide in a preclinical model of human breast cancer. *Oncotarget* **7**, 33306–33315 (2016).
25. E. Kenyon *et al.*, Ductal tree ablation by local delivery of ethanol prevents tumor formation in an aggressive mouse model of breast cancer. *Breast Cancer Res.* **21**, 129 (2019).
26. G. Wang *et al.*, Intraductal fulvestrant for therapy of ERα-positive ductal carcinoma in situ of the breast: A preclinical study. *Carcinogenesis* **40**, 903–913 (2019).
27. M. K. Joseph *et al.*, Intraductal drug delivery to the breast: Effect of particle size and formulation on breast duct and lymph node retention. *Mol. Pharm.* **17**, 441–452 (2020).
28. F. Al-Zubaydi *et al.*, Breast intraductal nanoformulations for treating ductal carcinoma in situ II: Dose de-escalation using a slow releasing/slow bioconverting prodrug strategy. *Drug Deliv. Transl. Res.* **12**, 240–256 (2022).
29. G. Sflomos *et al.*, A preclinical model for ERα-positive breast cancer points to the epithelial microenvironment as determinant of luminal phenotype and hormone response. *Cancer Cell* **29**, 407–422 (2016).
30. A. Ghosh *et al.*, MIND model for triple-negative breast cancer in syngeneic mice for quick and sequential progression analysis of lung metastasis. *PLoS One* **13**, e0198143 (2018).
31. F. Kittrell *et al.*, Mouse mammary intraductal (MIND) method for transplantation of patient derived primary DCIS cells and cell lines. *Bio Protoc.* **6**, e1744 (2016).
32. C. Alewine, R. Hassan, I. Pastan, Advances in anticancer immunotoxin therapy. *Oncologist* **20**, 176–185 (2015).
33. M. Dieffenbach, I. Pastan, Mechanisms of resistance to immunotoxins containing *Pseudomonas* exotoxin A in cancer therapy. *Biomolecules* **10**, 979 (2020).
34. J. K. Batra *et al.*, Antitumor activity in mice of an immunotoxin made with anti-transferrin receptor and a recombinant form of Pseudomonas exotoxin. *Proc. Natl. Acad. Sci. U.S.A.* **86**, 8545–8549 (1989).
35. H. Shinohara *et al.*, Site-specific expression of transferrin receptor by human colon cancer cells directly correlates with eradication by antitransferrin recombinant immunotoxin. *Int. J. Oncol.* **17**, 643–651 (2000).
36. A. Antignani *et al.*, Targeting receptors on cancer cells with protein toxins. *Biomolecules* **10**, 1331 (2020).
37. L. Jacobs, S. Sukumar, V. Stearns, Intraductal therapy for the prevention of breast cancer. *Curr. Opin. Investig. Drugs* **11**, 646–652 (2010).
38. M. E. Mahoney *et al.*, Intraductal therapy of ductal carcinoma in situ: A presurgery study. *Clin. Breast Cancer* **13**, 280–286 (2013).
39. X. W. Kuang *et al.*, Intraductal therapy in breast cancer: Current status and future prospective. *J. Mammary Gland Biol. Neoplasia* **25**, 133–143 (2020).
40. J. Wei *et al.*, Recombinant immunotoxins with albumin-binding domains have long half-lives and high antitumor activity. *Proc. Natl. Acad. Sci. U.S.A.* **115**, E3501–E3508 (2018).

41. C. P. Theuer, R. J. Kreitman, D. J. FitzGerald, I. Pastan, Immunotoxins made with a recombinant form of *Pseudomonas* exotoxin A that do not require proteolysis for activity. *Cancer Res.* **53**, 340–347 (1993).
42. T. N. Aung *et al.*, A new tool for technical standardization of the Ki67 immunohistochemical assay. *Mod. Pathol.* **34**, 1261–1270 (2021).
43. C. Marinaccio, D. Ribatti, A simple method of image analysis to estimate CAM vascularization by APERIO ImageScope software. *Int. J. Dev. Biol.* **59**, 217–219 (2015).
44. J. Schindelin *et al.*, Fiji: An open-source platform for biological-image analysis. *Nat. Methods* **9**, 676–682 (2012).
45. H. Bergholtz *et al.*; Oslo Breast Cancer Research Consortium (OSBREAC), Contrasting DCIS and invasive breast cancer by subtype suggests basal-like DCIS as distinct lesions. *NPJ Breast Cancer* **6**, 26 (2020).
46. M. P. DiGiovanna *et al.*, Active signaling by HER-2/neu in a subpopulation of HER-2/neu-overexpressing ductal carcinoma in situ: Clinicopathological correlates. *Cancer Res.* **62**, 6667–6673 (2002).
47. M. D. Ryser *et al.*, Incidence of ductal carcinoma *In Situ* in the United States, 2000–2014. *Cancer Epidemiol. Biomarkers Prev.* **28**, 1316–1323 (2019).
48. A. V. Barrio, K. J. Van Zee, Controversies in the treatment of ductal carcinoma in situ. *Annu. Rev. Med.* **68**, 197–211 (2017).
49. E. Provenzano, S. E. Pinder, Modern therapies and iatrogenic changes in breast pathology. *Histopathology* **70**, 40–55 (2017).
50. Y. Shen *et al.*, Transferrin receptor 1 in cancer: A new sight for cancer therapy. *Am. J. Cancer Res.* **8**, 916–931 (2018).
51. W. Wang *et al.*, IRP2 regulates breast tumor growth. *Cancer Res.* **74**, 497–507 (2014).
52. J. J. Going, D. F. Moffat, Escaping from Flatland: Clinical and biological aspects of human mammary duct anatomy in three dimensions. *J. Pathol.* **203**, 538–544 (2004).
53. M. Flanagan, S. Love, E. S. Hwang, Status of intraductal therapy for ductal carcinoma in situ. *Curr. Breast Cancer Rep.* **2**, 75–82 (2010).
54. S. M. Love *et al.*, A feasibility study of the intraductal administration of chemotherapy. *Cancer Prev. Res. (Phila.)* **6**, 51–58 (2013).
55. D. Rodin *et al.*, Long-term outcomes of women with large DCIS lesions treated with breast-conserving therapy. *Breast Cancer Res. Treat.* **192**, 223–233 (2022).
56. T. J. O'Keefe, O. Harismendy, A. M. Wallace, Large and diffuse ductal carcinoma in situ: Potentially lethal subtypes of "preinvasive" disease. *Int. J. Clin. Oncol.* **27**, 121–130 (2022).